Journal of Road Engineering 5 (2025) 452–466

Contents lists available at ScienceDirect

Journal of Road Engineering

journal homepage: www.keaipublishing.com/en/journals/journal-of-road-engineering

Original Article

Tire/road noise analysis of innovative microsurfacing mixtures based on SPERoN® model and noise-related texture indicators

Sérgio Copetti Callai [a], Manuel De Rose [b,*], Beate Altreuther [c], Rosolino Vaiana [b], Cesare Sangiorgi [a]

[a] Department of Civil, Chemical, Environmental and Materials Engineering, University of Bologna, Bologna 40136, Italy
[b] Department of Civil Engineering, University of Calabria, Rende 87036, Italy
[c] Mueller-BBM Industry Solutions GmbH, Planegg 82152, Germany

HIGHLIGHTS

- Six novel microsurfacing mixture were formulated by combining basalt, crumb rubber and artificial aggregates.
- The SPERoN® model was used to analyse the vibro-dynamic and aerodynamic components of rolling noise.
- Using a lower nominal maximum aggregate size and uniformly shaped artificial aggregates enhances pavement acoustic features.
- The *g*-factor derived from the Abbott curve effectively assess road pavement noise.
- This study highlights how mix design choices impact rolling noise, enabling the development of improved low-noise surfaces.

ARTICLE INFO

Keywords:
Tire/road noise
Pavement surface texture
SPERoN model
Bituminous microsurfacing
Geopolymer aggregates
Crumb rubber

ABSTRACT

Road traffic noise is a significant environmental issue in urban areas with major health and economic implications for communities. Thus, a comprehensive understanding of tire/road noise mechanism is crucial for road pavement engineering. This study evaluates the noise behaviour of six innovative microsurfacing mixtures incorporating natural and artificial aggregates (geopolymers and crumb rubber) with varying particle size distributions and binders. A 2D laser analysis aims at collecting surface texture indicators, while noise-related indicators were derived according to ISO 10844 standards. Noise levels were predicted using the SPERoN® model (statistical physical explanation of rolling noise), analysing the vibro-dynamic and the aerodynamic contributions separately. Correlations between tire/road noise levels predicted by the model and surface texture indicators elucidate the key factors influencing noise generation mechanism. The findings indicate that lower nominal maximum aggregate size (NMAS) and uniformly shaped artificial aggregates substantially mitigate rolling noise. Moreover, profiles with negative skewness and positive kurtosis exhibit reduced noise generation. The study highlights the limitations of traditional indicators like the estimated noise difference due to texture (END_T) and highlights the *g*-factor from the Abbott curve as a more reliable predictor of pavement noise properties. These findings provide valuable insights for designing low-noise pavements with enhanced performance, offering new perspectives on the noise behaviour and acoustic properties of microsurfacing.

1. Introduction

The rapid pace of urbanization has led to a significant rise in noise pollution levels, severely impacting quality of life and contributing to various physical and mental health disorders in humans. Notably, researches have established a connection between noise pollution and cardiovascular disease (Descornet, 2006; European Environment Agency, 2020; Münzel et al., 2021), hypertension (Pyko et al., 2018), sleep deprivation, and depression and anxiety (Beutel et al., 2020). Furthermore, studies suggest that noise pollution can negatively impact

* Corresponding author.
E-mail addresses: callai@isac.rwth-aachen.de (S. Copetti Callai), manuel.derose@unical.it (M. De Rose), beate.altreuther@mbbm-ind.com (B. Altreuther), rosolino.vaiana@unical.it (R. Vaiana), cesare.sangiorgi4@unibo.it (C. Sangiorgi).
Peer review under responsibility of Chang'an University.

https://doi.org/10.1016/j.jreng.2025.05.001
Received 23 September 2024; Received in revised form 3 March 2025; Accepted 5 May 2025
Available online 14 July 2025

stress levels during pregnancy and child development (Christensen et al., 2016; Zhang et al., 2021). In addition to health implications, noise pollution imposes significant economic costs, including increased healthcare expenses, reduced productivity, property devaluation, and direct expenses associated with noise mitigation strategies (e.g., building noise barriers) (European Comission,; Eelco den Boer and Schroten, 2007; Pignier, 2015). Notably, noise affects less socio-economically advantaged groups who are often exposed to higher levels (Dreger et al., 2019; European Environment Agency, 2020). The European Environment Agency (EEA) estimates that road traffic noise is the most prevalent source, exceeding exposure to rail, aircraft, and industrial noise, with over 113 million people subjected to noise levels exceeding 55 dB (European Environment Agency, 2020).

Traffic noise originates from a combination of several factors, including aerodynamic noise generated by the vehicle's shape, propulsion noise from the power unit, and tire/road noise (rolling noise) arising from the interaction between tires and the road surface (Praticò, 2014; Ma et al., 2024). While aerodynamic noise is only significant at very high speeds, propulsion noise becomes more relevant at low speeds and for heavy vehicles. On the contrary, in the mid-to-high speed range (around 35 km/h for cars and 75 km/h for trucks), rolling noise dominates as the primary source (Chen et al., 2021a; Mikhailenko et al., 2022). In response to rising traffic noise concerns, the automotive industry has been studying various strategies for modern vehicles, including the development of quieter vehicle shapes and engines (e.g., electric vehicles) (Poulikakos et al., 2022). However, these solutions offer only partial mitigation of the overall traffic noise issue. Therefore, to achieve comprehensive control of road noise pollution, it becomes fundamental to assess the tire/road noise component, a major part of which is highly dependent on the pavement texture characteristics (Gottaut and Goubert, 2016). The tire/road noise generation arises from the combination of two key phenomena: the vibro-dynamic noise and the aerodynamic noise. Vibro-dynamic noise, dominant at frequencies below 1 kHz, originates from the mechanical impacts between the tire and the road surface irregularities. On the other hand, aerodynamic phenomena are dominant at frequencies higher than 1 kHz (Del Pizzo et al., 2020; Ling et al., 2021).

Furthermore, considering the different domains of surface texture, rolling noise is associated with the macrotexture and megatexture domains, with wavelengths, λ in the range of 0.5–50 mm and 50 mm to 0.5 m, respectively (Praticò and Vaiana, 2015). Nonetheless, tire characteristics are closely linked to stringent safety, durability, and fuel consumption standards, minimizing the scope for optimizing noise generation characteristics. This emphasizes the importance of designing low-noise pavements and optimizing the surface texture to reduce tire/road noise (Altreuther and Maennel, 2018; Leng et al., 2023; Vaiana et al., 2023).

Among different solutions, it is worth to mention the low-noise stone mastic asphalt (SMA) obtained by using a modified grading curve with 9%–13% of air voids and higher binder content to improve its acoustic performance (Zakerzadeh et al., 2024). Open-graded asphalt pavements, such as open graded friction course and twin layers, are associated with a good acoustic absorption due to the intrinsic porosity of the layer, whereas porous elastic road surfaces (PERS) reduce the production of rolling noise due to their higher presence of interconnected voids and an inherent low-stiffness (presence of crumb rubber) (Goubert et al., 2016; Li et al., 2024; Vázquez et al., 2020). However, these solutions have a higher cost, due to the presence of high-quality aggregates and polymer-modified binders, which makes them economically suitable only when applied in noise-sensitive areas (JRE Editorial Office et al., 2023; Praticò, 2014).

In contrast, dense road surfaces, due to their lack in porosity, can provide noise reduction by means of acoustically optimized surface texture. Road surfaces with low nominal maximum aggregate size (NMAS) (Praticò and Briante, 2020) provide level surfaces with relatively low thickness. In the last decades, one of the most researched pavement maintenance strategy without structural functions is microsurfacing. This technique enhances skid resistance and exhibits a pronounced surface texture, providing a smooth layer that adheres to the underlying pavement, seals cracks, and protects against water infiltration (Bhargava et al., 2020a; Li et al., 2017; Tan et al., 2023; Xu et al., 2024). Microsurfacing involves applying a mixture of polymer-modified bituminous emulsion, cement, water, and mineral aggregates with a maximum size of 8–10 mm, typically at thicknesses not exceeding 10 mm (Bhargava et al., 2020b; Grilli et al., 2019). Knowledge of rolling noise generated by the interaction between tires and microsurfacing pavements remains limited. However, some research suggests that their rough macrotexture, resulting from the absence of compaction during the application process, induces tire vibration phenomena, which are responsible for noise production. In contrast, other studies demonstrate that noise emissions from microsurfacing layers are comparable, or in some cases even better, than those from conventional hot-mix asphalt (HMA) (Li et al., 2012) and SMA pavements (De Rose et al., 2023; Nowoświat et al., 2020). Furthermore, the manipulation of the aggregate gradation or the incorporation of crumb rubber in the mixture could also lead to a reduction in noise emissions (Canestrari et al., 2009; Chen et al., 2021b; Sangiorgi et al., 2012).

Besides, it is evident that studies aiming to reduce pavement noise require robust validation. Therefore, to deepen the understanding of noise generation mechanisms and optimize low-noise pavement designs, various predictive models have been developed to simulate tire/road noise behaviour under different conditions, either based on numerical, statistical or analytical approach. For example, Kleizienė et al. (2019) developed a multiple linear model to predict CPX based on mixture composition, including parameters such as granulometry, bitumen content, and void volume. However, this model is limited to a specific speed (80 km/h) and does not account for the frequency spectrum. Similarly, Teti et al. (2020) focused on developing a model for rolling noise based on the mixture job mix formula, achieving accurate CPX level predictions across different frequency ranges (low, medium, and high). Nevertheless, the model does not consider the absorption properties of the investigated pavement type. Chen et al. (2018) proposed a semi-empirical model for evaluating the rolling noise of porous asphalt mixtures. Their approach incorporates surface texture (disaggregated through texture level, L_{TX}) and accounts for noise absorption properties by modelling the voids within the mixture and their interconnections. However, these studies predict noise levels without considering the physical interaction at the tire-pavement contact.

The calculation model SPERoN® (statistical physical explanation of rolling noise) applied in the current project is a hybrid modelling framework to predict the pass-by level of vehicles, using road surface texture profiles and tire data as input. SPERoN® combines a physical and a statistical sub-model by considering different noise generation mechanisms contributing to tire/road noise. The model was proposed and developed by M+P, Müller-BBM and the Division of Applied Acoustic of the Chalmers University Gothenburg (Beckenbauer and Kuijpers, 2001), based on measurements of pass-by noise and road surface texture on a multitude of different surfaces, of mechanical characteristics of different tires and on theoretical investigations considering aerodynamic noise. The SPERoN® model was validated in the P2RN-project (Beckenbauer et al., 2008; Klein et al., 2008) to predict pass-by levels of passenger cars with an accuracy of ±1 dB. The model was used in several European projects such as SILVIA (Descornet, 2006) and ITARI (Beckenbauer et al., 2008; Berge et al., 2009; Rahmani et al., 2011) for developing low noise road surfaces. Whether used independently (Poulikakos et al., 2024) or in combination with auralization tools to enable realistic reproduction of specific acoustic conditions for evaluating psychoacoustic perception (Forssén et al., 2018; Hoffmann and Kropp, 2019), the SPERoN® model has supported the development of low-noise pavements since its introduction (Peeters et al., 2024).

Based on the findings of the literature review, the main objective of this research is confined in the investigation of the acoustic performance

of six innovative microsurfacing mixtures with varying natural and artificial aggregate compositions, binder types, and particle size distributions. In particular, the most widely surface texture indicators, together with noise-related indicators according to the ISO 10844 standard, were calculated and compared to tire/road noise levels in a pass-by situation obtained through the use of the SPERoN® prediction model. The goal is to identify correlations between pavement texture properties and rolling noise generation mechanisms, thereby enhancing the design of low-noise pavements and providing insights for optimizing texture parameters to reduce traffic noise effectively.

2. Materials and methods

The research is structured into four steps.

(1) Mixture preparation and profile readings by means of a laser profilometer;
(2) Surface texture analysis to derive both aggregate and spectral texture indicators, and noise-related indicators in accordance with the ISO 10844 standards;
(3) Noise modeling with SPERoN® to assess the noise produced by the different mixtures encompassing both tire-vibration and aerodynamic noise contributions;
(4) Analysis of results, including a comparative evaluation between the individual outcomes of the two approaches (prediction models and texture indicators), to identify potential correlations that explain the noise phenomena associated with road pavements.

In the following paragraphs, the abovementioned key points of the research will be elaborated in greater detail. In particular, a complete flowchart of the paper's experimental plan is proposed in Fig. 1.

2.1. Microsurfacing samples

Cold bituminous microsurfacing mixtures were manufactured using various combination of aggregates and binder type. In particular, basalt aggregates were used as natural aggregates, whereas crumb rubber (CR), of mesh size 0.8/4.0 mm, and artificial engineered aggregates (AEA), of 10 mm single size, were used as aggregates substitutes of natural ones.

Notably, the AEAs were produced using an alkali-activation technique (geopolymers), presented and evaluated in a parallel study (Copetti Callai et al., 2022). The mortar, consisting in a mixture of basalt powder and metakaolin with an activator (alkali solution), is set into 3D printed molds and cured in the oven, producing final AEA with 10 mm diameter in a truncated octahedron shape, as shown in Fig. 2.

The type of binders used were asphalt emulsion modified with latex and a non-bituminous resin emulsion. Finally, following the ISSA mix design specification (ISSA, 2010), six different samples were produced, summarized in Table 1.

The compositional design of the mixtures aimed to achieve varied surface textures, each expected to exhibit distinct noise generation behaviours. The samples NAS1 and NAS2 represent two reference microsurfacing mixtures, specifically designed with tailored particle size distributions (0/8 mm) of basalt aggregates as part of the project of the TG2 working group within the RILEM technical committee 280-CBE. Building upon this distribution, the rubber sample was developed by replacing a portion of the aggregate with 60% of CR. The particle size distribution of mixture AA adhered to Australian guidelines (Patrick, 2018), featuring a larger NMAS compared to the NAS samples, and substituting basalt aggregates with AEAs in the upper sieve size (9.5 mm). Finally, the Yellow mixture, which also employs a RILEM-specific particle size distribution, features a finer gradation (0/6 mm). The fine fraction (0/2 mm) of this latter was blended in a 50:50 ratio with AEAs to produce sample AA5050. The particle size distributions of the mixtures are shown in Fig. 3.

Other information regarding the materials used can be found in a previous work (Callai et al., 2022). In Fig. 4, the six produced samples are shown. Once the samples cured, the texture analysis was conducted

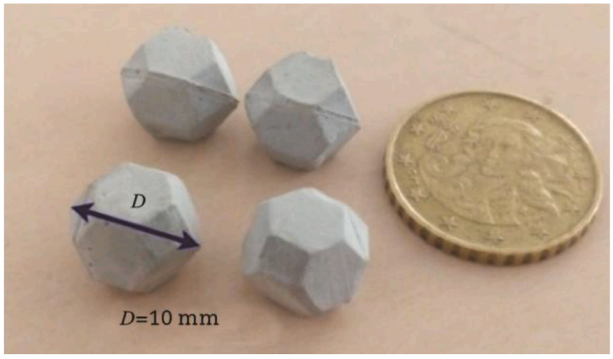

Fig. 2. Sample of artificial engineered aggregates (AEA).

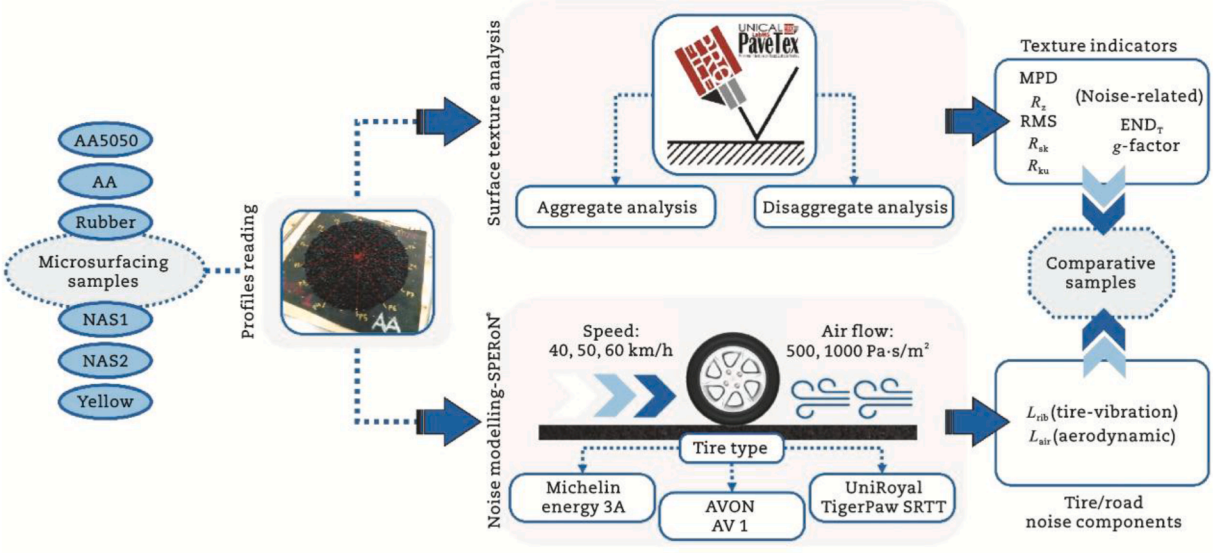

Fig. 1. Schematic representation of the variables and workflow.

Table 1
Compositional design of the studied mixtures.

Sample name	Particle size distribution	Binder type
AA5050	• 50% <sieve 2 mm of 0/6 mm RILEM • 50% 10 mm AEAs	Asphalt emulsion modified with latex
AA	• 0/10 mm Australian guidelines • Replacing sieve 9.5 mm with AEAs (10%)	Asphalt emulsion modified with latex
Rubber	• 40% of 0/8 mm RILEM • 60% of 0.8/4 mm CR	Asphalt emulsion modified with latex
NAS1	• 0/8 mm RILEM	Asphalt emulsion modified with latex
NAS2	• 0/8 mm RILEM	Asphalt emulsion modified with latex
Yellow	• 0/6 mm RILEM	Non-asphaltic resin

by means of a contactless laser profilometer (ISO 13473-3) (ISO, 2002). The laser profilometer conducted seven radial reads, summing up to 2 m of linear profile to ensure its representativeness. The yellow markers on each sample shown in Fig. 4 represent the acquired profiles.

2.2. Texture evaluation

The surface texture can be described as the sum of various elementary components, each corresponding to a specific wavelength: in particular, the surface macrotexture falls within the range of wavelengths between 0.5 and 50 mm. There exists a plurality of geometric indicators, not necessarily related to specific wavelengths, which effectively characterize the surface texture and can be derived through simple computation on the profile data (distances x and heights z) from a two-dimensional point of view (Callai et al., 2022; Chen et al., 2022). Within the broader spectrum of available indicators, this investigation will place particular emphasis on the mean profile depth (MPD), the average peak-to-valley height, R_z, the root mean square, RMS, the skewness, R_{sk}, and the kurtosis, R_{ku}.

(1) Mean profile depth (MPD)

The most widely used parameter to describe the pavement macrotexture is the MPD, which, according to the ISO 13473–1:2019 (ISO, 2019), represents the average value of the profile depth within a sampling length of 100 mm (baseline) for a given profile curve (Puzzo et al., 2017). Specifically, this baseline (and therefore the profile) is divided into two parts and the MPD is calculated as the difference between the average peak height of the two individual parts (h_1 and h_2) and the central line height (h), as provided in Eq. (1).

$$\mathrm{MPD} = \frac{h_1 + h_2}{2} - h \tag{1}$$

(2) Average peak-to-valley height (R_z)

The statistic R_z reflects the overall roughness of a surface profile and represents the average of the maximum peak-to valley heights measured over five contiguous samples of a specified length and along a defined sampling length of 100 mm (Boscaino and Pratico, 2001). Thus, it is computed as the average height of the top five peaks (Z_{pi}) to the average depth of the top five valleys (Z_{vi}) within a measured length, as shown in Eq. (2).

$$R_z = \frac{1}{5}\sum_{i=1}^{n} Z_{pi} - Z_{vi} \tag{2}$$

(3) Root mean square (RMS)

The RMS of the profile is basically the root mean square of the profile's deviation (Eq. (3)), being very sensitive to the presence of peaks and valleys (Boscaino and Pratico, 2001). This parameter becomes quantitatively more relevant as the wave amplitude increases, but it is not sensitive to changes in wavelength.

$$\mathrm{RMS} = \sqrt{\frac{1}{L}\int_0^L (z - \bar{z})^2 \mathrm{d}x} \tag{3}$$

(4) Skewness (R_{sk})

The Skewness quantifies the asymmetry of a profile's height distribution, reflecting how peaks and valleys are positioned relative to the average value (Tayebi and Polycarpou, 2004; Zhan and Huang, 2019). When $R_{sk} = 0$, it indicates a symmetrical distribution, where peaks and valleys balance out around the average. A negative skewness suggests

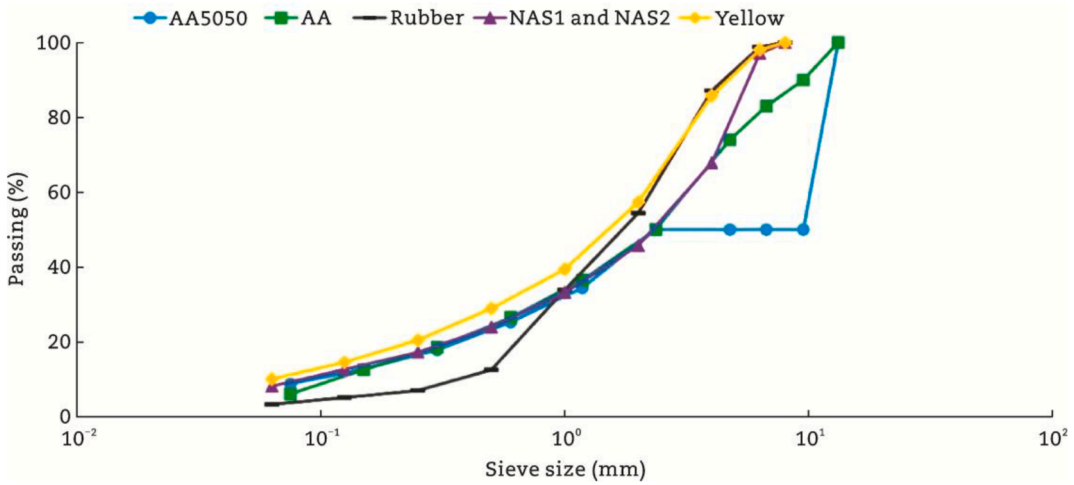

Fig. 3. Particle size distributions of the Microsurfacing mixtures.

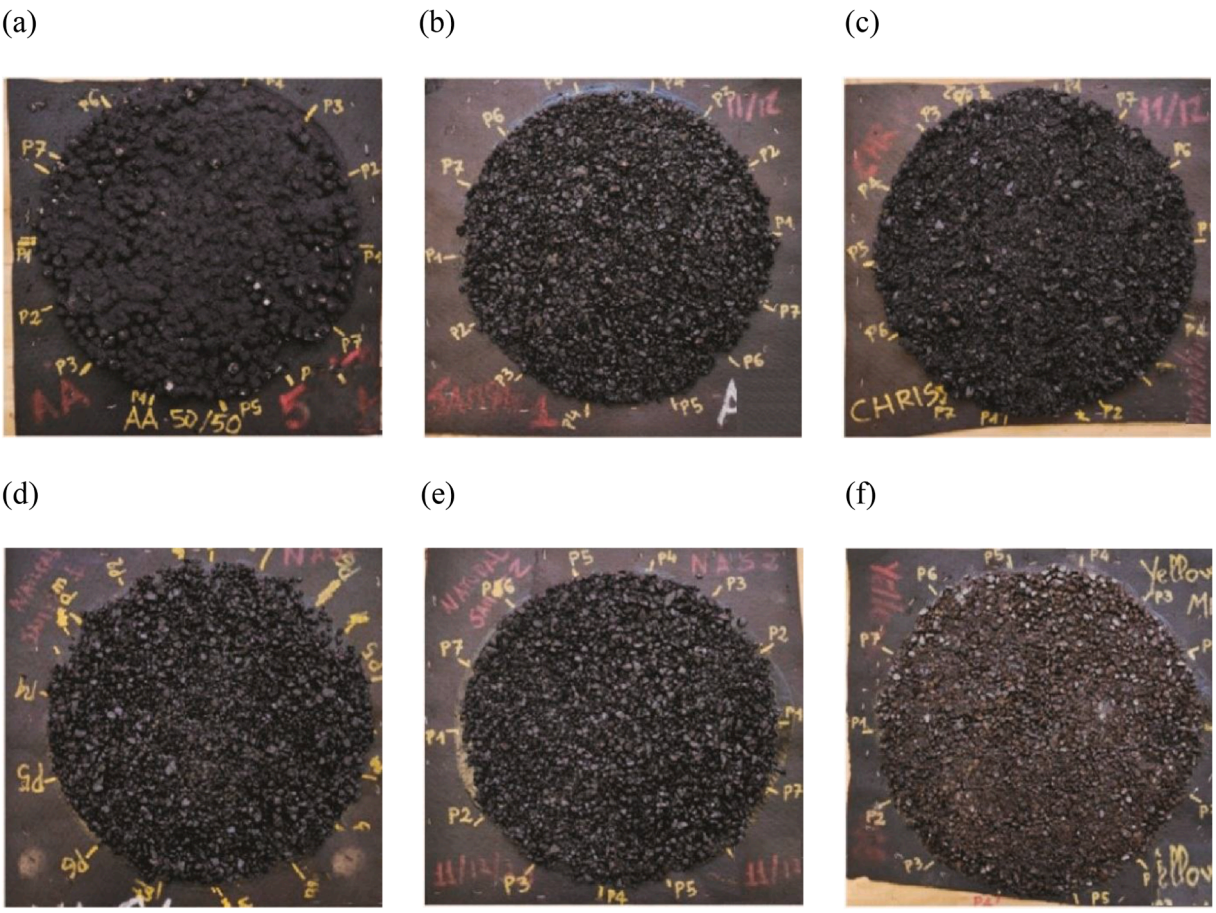

Fig. 4. Microsurfacing samples. (a) AA5050. (b) AA. (c) Rubber. (d) NAS1. (e) NAS2. (f) Yellow.

more frequent peaks above the average, with a longer tail on the left side of the distribution; conversely, a positive skewness indicates more frequent valleys below the average, with a longer tail on the right side (Eq. (4)).

$$R_{sk} = \frac{\sum_{i=1}^{n} \frac{1}{n} (z_i - \bar{z})^3}{\left(\sum_{i=1}^{n} \frac{1}{n} (z_i - \bar{z}) \right)^{3/2}} \tag{4}$$

(5) Kurtosis (R_{ku})

Kurtosis describes the "peakedness" of the probability density function (Eq. (5)). It compares the distribution's shape to a normal curve (having a kurtosis equal to 0): if R_{ku} is greater than 0, the distribution is more peaked, thus suggesting that values are concentrated around the mean; on the contrary, for values lower than 0, the distribution is flatter with more dispersed values (Vieira et al., 2021; Zhan and Huang, 2019).

$$R_{ku} = \frac{\sum_{i=1}^{n} \frac{1}{n} (z_i - \bar{z})^4}{\left(\sum_{i=1}^{n} \frac{1}{n} (z_i - \bar{z})^2 \right)^2} \tag{5}$$

The surface texture data described above were obtained through the acquisition and post-processing of longitudinal profiles identified on the produced microsurfacing samples. Specifically, the analysis of the profiles was carried out using a laser profilometer based on conoscopic holography. To ensure good statistical representation, seven equally spaced diametral profiles, each 30 cm in length, were captured for each sample. The profiles were analysed using the U-PaveTex software developed by the University of Calabria, which computed the desired indicators (i.e., MPD, R_z, etc.), while skewness and kurtosis were calculated using Microsoft Excel. The software additionally calculates the texture level, $L_{TX,\lambda}$, of the analysed profiles, which represents the logarithmic transformation of the profile's amplitude for a given wavelength, λ.

2.3. Noise related indicators

The international standard ISO 10844 (ISO, 2014, 2021) "acoustics – specification of test tracks for measuring sound emitted by road vehicles and their tyres", which specifies the characteristics of a test track surface intended to be used for measuring rolling noise caused by the tire/-pavement interaction, provides in its different versions noise related texture indicators. According to the literature, these indicators may be used as descriptors of the acoustic properties related to the surface texture. Indeed, although the calculation of these indicators is not mandatory, they may be used as an analytical approach to understand the noise behaviour of the pavements.

(1) Estimated pass-by noise level difference from texture level variations (END_T)

The first indicator introduced as single parameter for evaluating the texture effect on noise is the END_T, which was developed within the SILVIA project (Descornet, 2006) and considered in the ISO 10844:2014 (ISO, 2014). This method uses the one-third-octave band wavelength spectrum of a surface, with λ ranging from 5 to 100 mm, and compares it to a reference spectrum, provided by the standard. The spectral differences are then weighted with coefficients that define the relevance of each spectral band for the rolling noise in the corresponding

one-third-octave band. These differences are further weighted based on an average rolling noise spectrum, producing a single value that estimates the difference in rolling noise level compared to the reference (van Blokland and Schwanen, 2012). In accordance with the standard, the calculation of END_T is presented in Eq. (6).

$$END_T = 10\log_{10}\left(\frac{\sum_i 10^{\frac{L_{mi}+b_i\Delta L_{TX,i}}{10}}}{\sum_i 10^{\frac{L_{mi}}{10}}}\right) - 0.25\Delta L_{TX,5} \quad (6)$$

where L_{mi} are reference noise levels, b_i are fixed factors, $\Delta L_{TX,5}$ is the difference between the measured texture level of the surface under consideration for the texture wavelength 5 mm and a reference texture level for the wavelength 5 mm, equal to 39.8 dB; in particular, the terms L_{mi} and b_i can be found in the standard ISO 10844:2014 (ISO, 2014), Annex A.

(2) Shape-factor (*g*-factor)

The recently published ISO 10844:2021 (ISO, 2021) standard has supplanted the END_T, introducing a new parameter, the shape factor (*g*-factor), to correlate surface texture with rolling noise generation. The *g*-factor is typically determined from the cumulative frequency distribution (Abbott-Firestone curve) of the surface profile depths. It represents the cumulative frequency corresponding to half of the maximum profile depth (ISO 10844: 2021 (ISO, 2021)). This value reflects the percentage of material (cumulative distribution) included between the highest peak and the half of the maximum peak to valley height. Consequently, the *g*-factor provides valuable insight regarding the surface texture shape and exhibits a strong correlation with pavement surface acoustics: a higher shape factor corresponds to a reduction in the noise emission (Miljković and Radenberg, 2012). Generally, a shape factor higher than 70% is associated with surfaces characterized by negative texture, whereas positive textures typically exhibit *g*-factor values below 50% (Miljković et al., 2014). According to Eqs. (7) and (8), the *g*-factor corresponds to the cumulative distribution, D_{cum}, referred to the mid-point elevation, z_{mid}.

$$z_{mid} = \frac{z_{max} + z_{min}}{2} \quad (7)$$

$$D_{cum,i} = (i-1)\frac{100\%}{n-1} \quad (8)$$

2.4. Noise evaluation with SPERoN®

As stated in the introduction, the SPERoN® is a hybrid modelling framework for the simulation and prediction of tire/road noise that combines a physical and a statistical sub-model. The physical part aims at pre-processing the surface texture to identify the tire/road contact area, calculate the contact forces and the noise generated from tire vibrations, whereas the statistical parts are used for the prediction of airflow-related mechanisms such as the tire cavity noise and residual sound sources (mainly the aerodynamic noise around the car body) (Alves and Maennel, 2016). Through a series of multivariate linear regression models, SPERoN® is able to predict the coast-by noise levels in 1/3 octave band spectra emitted by a passenger car, given a certain tire/road combination. Given the above, the input data for the model are of two types: 1) road surface, this includes the surface texture profiles, collected by means of a laser profilometer and in a longitudinal direction, to build a quasi-3D surface texture, and the acoustical impedance of the surface; 2) tire, this includes the three-dimensional profile and the geometry of the tire, its radial stiffness, the width and the rolling speed (Kuijpers and Van Blokland, 2001).

Fig. 5 shows a schematic workflow of the SPERoN® model. Specifically, the model reproduces the absolute third-octave levels of coast-by spectra, with an accuracy of ±1 dB(A), achieved as a sum of four distinct contributions that can be calculated separately (Eq. (9)).

$$p^2_{coast\text{-}by} = p^2_{vib} + p^2_{air} + p^2_{cav} + p^2_{residual} \quad (9)$$

where p_{vib} represents the mechanically sound source component caused by the interaction of contact forces between the tire and the pavement

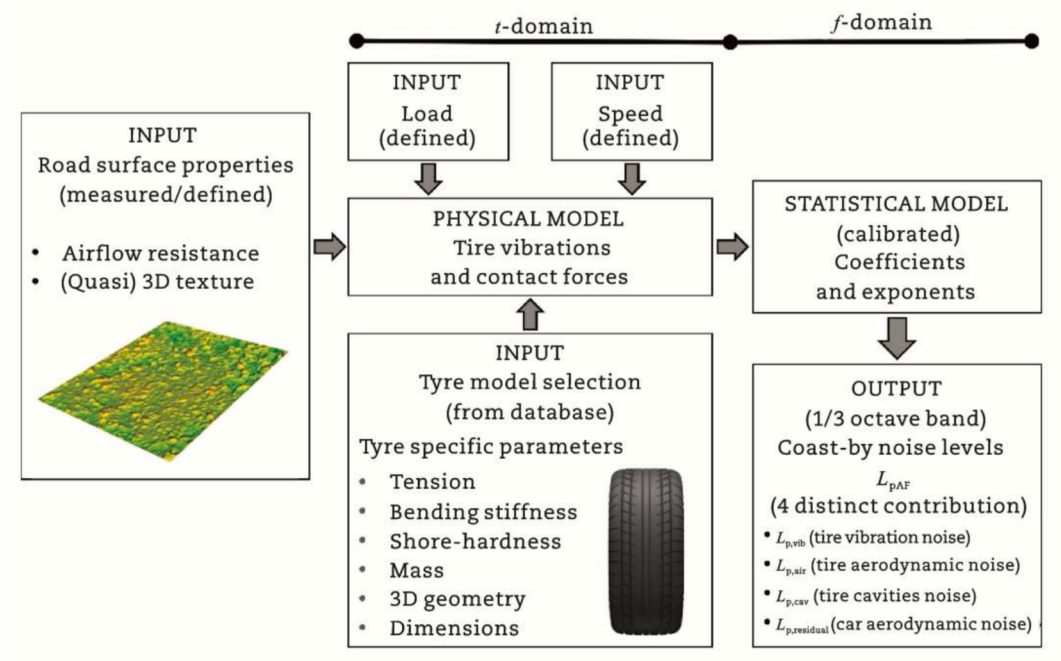

Fig. 5. Schematic workflow of SPERoN model adapted from Beckenbauer et al. (2008).

(Eq. (10)), p_{air} is related to the aerodynamic contribution arising within the tire-road contact (Eq. (11)), p_{cav} is the component arising from the resonance within the tire cavities (Eq. (12)), $p_{residual}$ is the aerodynamic noise due to the shape of the vehicle used for the analysis (Eq. (13)). Further details can be found in Beckenbauer et al. (2008).

$$p_{vib}^2 = aF_c^2 \Gamma^{\alpha 1} B^{\alpha 2} S^{\alpha 3} \tag{10}$$

$$p_{air}^2 = b\left(F_c^2 \Gamma^{-1.5} S^{-2}\right)^{\beta 1} B^{\alpha 2} V^4 \tag{11}$$

$$p_{cav}^2 = cG_{pattern}^{\gamma 1} \tag{12}$$

$$p_{residual}^2 = dV^{\delta 1} \tag{13}$$

where a, b, c, d are regression coefficients per third-octave band, $\alpha 1$, $\alpha 2$, $\alpha 3$, $\beta 1$, $\gamma 1$ and $\delta 1$ are real-valued exponents, F_c is the contact force in N, Γ is the tire/road contact air flow resistance in Pa · s/m, B is the tire width in m, S is the tire tread stiffness in N/m, $G_{pattern}$ is the spectral power of the tire's tread pattern variation; V is the speed in m/s.

In regard of road surface input, it should be noted that the development of SPERoN® was originally not aimed at the calculation with texture profiles shorter than the circumference of a standard tire. In the case of texture measurements on laboratory samples, where the texture profile length is shorter, the calculation with SPERoN® can only cover a limited frequency range, which means that it is impossible to predict realistic pass-by levels from laboratory sample profiles with SPERoN®. Therefore, in this research the SPERoN® model was only used to predict the two main components of tire/road noise, namely the tire/vibration noise level (L_{vib} (see p_{vib})) and the aerodynamic noise level (L_{air} (see p_{air})) for a direct comparison of the different mixes under investigation; moreover, the components p_{cav} and $p_{residual}$ are system invariants, as they are not influenced by the surface texture of the analysed samples. Given the above, the calculations were restricted to the frequency range of 400–2000 Hz. The airflow resistance in two different calculation runs was set to 500 and 1000 Pa · s/m^2, giving the lower and upper limit of realistic values. Regarding the tire, three types of tires were evaluated, summarised in Table 2, whose characteristics (Fig. 5) are included in the SPERoN® database. As the tires are commercially available, specific characteristics cannot be disclosed to safeguard proprietary information. For the sake of brevity, tire types will henceforth be identified solely by the manufacturer's name.

The Michelin tire was chosen as low noise tire, as the model calculations with this tire have been validated in the German-French P2RN project (German-French Cooperation P2RN, 2009). In addition, this tire has been investigated in several subsequent research projects yielding a considerable set of reference data. The Uniroyal tire is the standard reference test tire SRTT according to the UN ECE R117, an international standard regulating the technical and performance characteristics of tires for road vehicles, and widely used within the automotive industry. This latter is marked as louder than the Michelin tire. Finally, the AVON tire was considered because the production of noise associated with this type of tire is between the first two (Berge et al., 2009). The SPERoN® calculations were performed at three different rolling speeds (40, 50, and 60 km/h).

Table 2
Summary of the tires considered for the SPERoN application.

Manufacturer	Type	Dimension	Noise
Michelin	Energy 3A	195/60 R15	Low-noise
AVON	AV1	185/65 R15	Mid-level
UniRoyal	TigerPaw SRTT	225/60 R16	Loud

3. Results and discussions

3.1. Texture parameters and noise related indicators

The texture parameters and noise related indicators of each sample are presented in Table 3, respectively; note that each indicator is intended as the average of seven different profiles. Firstly, it is possible to notice that the smoother surfaces are the Yellow and the AA5050, showing the lowest MPD, R_z and RMS, with the minimal peak-to-valley heights. This could be attributable to the Yellow's lower particle size distribution and, on the other hand, to the AA5050 mixture's uniformity, with the presence of 50% of identically shaped AEAs. On the contrary, the highest values belong to the mixture AA, followed by the natural samples.

Secondly, it is worth noting that all the samples exhibit a slightly negative skewness, suggesting a tendency towards lower values compared to the average value of the profiles. Furthermore, kurtosis values mirror the trends observed for the previous indicators, where positive values indicate surfaces with profile heights (z_i) more evenly distributed around the mean, resembling a smoother surface. The Yellow mixture exhibited the highest kurtosis value, followed by AA5050. In contrast, NAS1, NAS2, and AA mixtures display negative kurtosis, while the Rubber mixture closely approximates a normal distribution of heights.

Regarding the noise-related indicators, significant differences are evident between the END_T and the g-factor of the various mixtures. While the g-factor appears to be consistent with the previously presented texture indicators, the same cannot be said for the END_T. It is important to recall that the END_T is derived from the difference between the texture spectra of the individual mixtures and the spectrum of an optimal surface. It is possible to state that the END_T indicator reflects their granulometric distribution, with Yellow exhibiting the lowest value due to its distribution with a lower NMAS. This is followed by the other mixtures, which show more or less comparable values, with the exception of the AA5050 mixture. Indeed, the higher presence of AEAs (10 mm aggregate size) in this mixture is not captured by this indicator. As for the g-factor, the highest value is associated with the Yellow mixture (82.1%), which consequently exhibits a negative texture, followed by the AA5050 and rubber mixtures (71.1% and 70.0%, respectively). The remaining mixtures show a g-factor close to 50%, indicating a positive texture.

3.2. Tire-vibration noise levels

The noise generated caused by the vibro-dynamic phenomena in the tire/road contact was evaluated for each sample at given airflow resistance and different speed. In particular, Fig. 6 shows the results for the Michelin tire (low noise), Fig. 7 resumes the results achieved by the AVON tire (medium noise) and Fig. 8 the Uniroyal tire (high noise).

Table 3
Texture and noise-related indicators for each sample.

Sample	MPD (mm)	R_z (mm)	RMS (mm)	R_{sk} (mm)	R_{ku} (mm)	END_T (dB(A))	g-factor (%)
AA5050	2.255	3.427	1.383	−0.657	1.079	5.357	71.1
AA	3.587	5.696	1.850	−0.007	−0.151	4.094	52.9
Rubber	2.631	4.463	1.896	−0.549	0.065	4.557	70.0
NAS1	3.054	4.617	1.776	−0.106	−0.446	3.966	55.7
NAS2	2.930	5.414	1.797	−0.133	−0.630	4.118	55.0
Yellow	1.971	3.082	1.108	−0.736	1.778	3.014	82.1

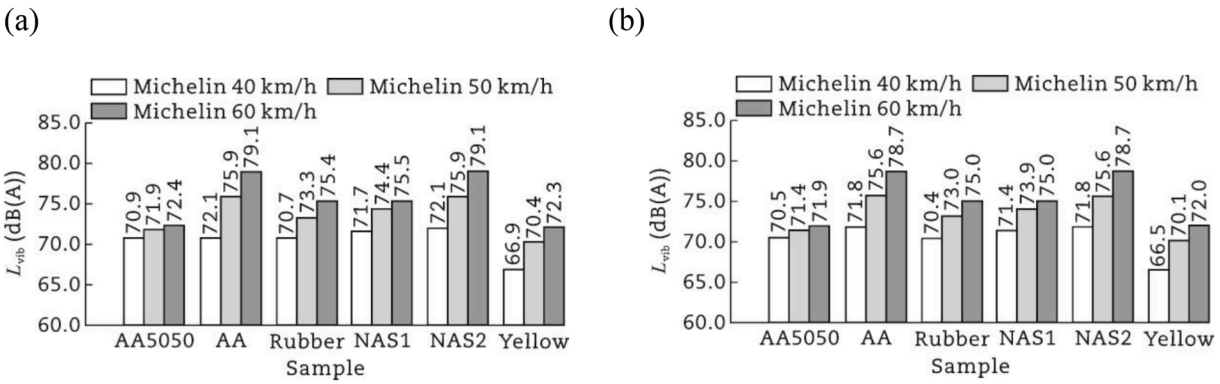

Fig. 6. L_{vib} noise levels for Michelin tire. (a) Air flow of 500 Pa · s/m^2. (b) Air flow of 1000 Pa · s/m^2.

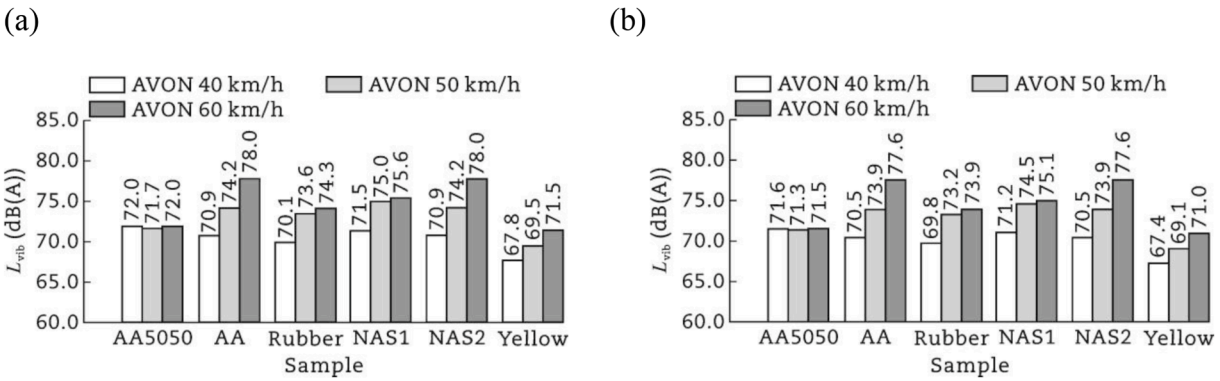

Fig. 7. L_{vib} noise levels for AVON tire. (a) Air flow of 500 Pa · s/m^2. (b) Air flow of 1000 Pa · s/m^2.

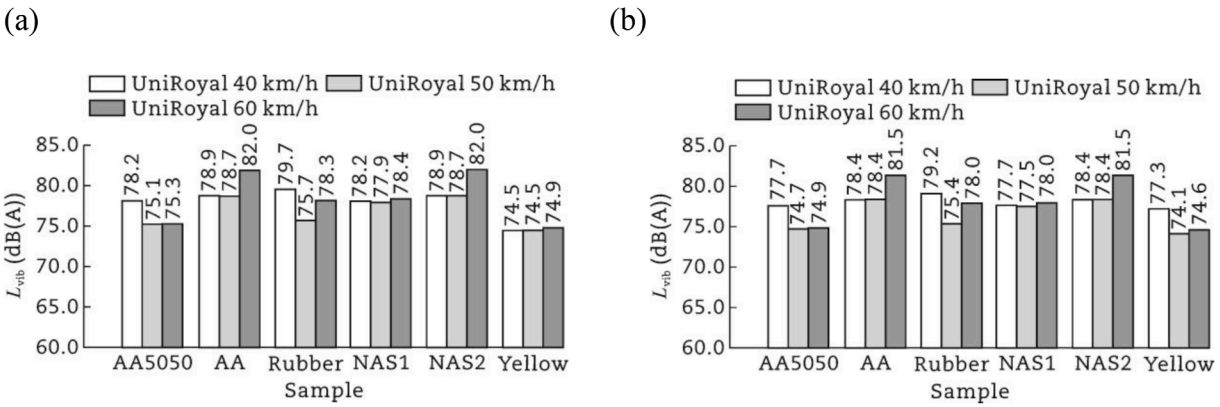

Fig. 8. L_{vib} noise levels for Uniroyal tire. (a) Air flow of 500 Pa · s/m^2. (b) Air flow of 1000 Pa · s/m^2.

As expected, the Uniroyal tire exhibits higher sound pressure levels compared to the other two tire types. Notably, the sound levels for the UniRoyal tire are consistently higher at 40 km/h than at 50 km/h, before rising again at 60 km/h. Indeed, the vibro-dynamic phenomenon is affected by multiple factors and, depending on the mechanical properties of the tire, sound levels can be higher when there is a resonance excitation or torus eigenmodes (Pinay et al., 2018); this behaviour does not necessarily occur at the highest speed investigated. Moreover, while the differences between low- and medium-noise tires are approximately 1–2 dB(A), the differences are significantly larger with respect to the Uniroyal tire, with variations reaching around 4–6 dB(A). No significant differences are observed between the various airflow resistances. However, for an airflow of 1000 Pa · s/m^2, sound levels are on average 0.3 dB(A) lower. For the same tire type and speed, it is worth noting that the Yellow mixture exhibits lower L_{vib} values compared to all other mixtures. In particular, the mixtures with Natural Aggregates and the AA mixture show largely comparable values, whereas Rubber performs slightly better. For this latter, it is worth to mention that the presence of crumb rubber could potentially contribute to reduce the noise levels due to its inherent stiffness and sound-absorption properties. In previous research, it has been demonstrated that such high amount of crumb rubber reduced the stiffness of the pavement (Makoundou et al., 2021a, 2021b); however, the model does not account the moduli of the analysed mixtures. Interestingly, the AA5050 mixture follows the Yellow mixture, but not at the lowest speed (40 km/h), where it becomes comparable to the other mixtures. As for the mixture AA, the presence of 10% of AEAs does not contributes in the reduction of noise levels.

3.3. Aerodynamic noise levels

The noise generated attributable to the air displacement in the tire/road noise, L_{air}, was evaluated for each tire, airflow pressure and according to the speed and sample. Fig. 9 shows the results of L_{air} noise for the Michelin tire (low noise), Fig. 10 for the AVON tire (medium noise) and Fig. 11 for the Uniroyal tire (high noise).

As expected, L_{air} values are generally lower than those attributed to vibro-dynamic noise, since aerodynamic phenomena are prevalent at speeds typically exceeding 60 km/h. In general, L_{air} values for the AVON tire are lower than those for the Michelin tire, while Uniroyal emerges as the noisiest tire. Airflow resistance plays a more significant role in the aerodynamic phenomena, with L_{air} values for an airflow resistance of 1000 Pa · s/m^2 being approximately 1 dB(A) lower than those for an airflow resistance of 500 Pa · s/m^2. Regarding the individual mixtures, surface texture appears to have a greater influence on the tire-vibration noise rather than aerodynamic phenomena, within the limitations of the analysis conducted in this study. Nevertheless, it is evident that the Yellow mixture exhibits lower sound pressure levels, followed by the AA5050 and rubber mixtures, and this holds true for all tire types, airflow resistances, and rolling speeds.

3.4. Noise spectra analysis

This paragraph provides a detailed characterization of the rolling noise components through the analysis of frequency spectra within the 400–2000 Hz range, a region of significant interest due to its alignment with human hearing sensitivity. Specifically, Fig. 12 illustrates the spectra of the vibro-dynamical noise, L_{vib}, whereas Fig. 13 presents the spectra of the aerodynamic noise, L_{air}, respectively for each sample and categorized for tire type and vehicle speed. Due to the minimal spectral differences between the two air flow values analysed with SPERoN®, the

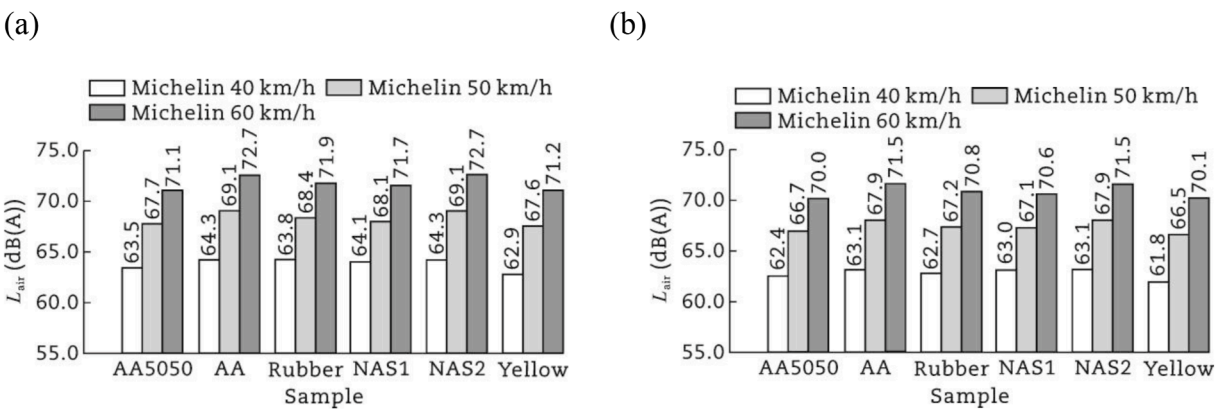

Fig. 9. L_{air} noise levels for Michelin tire. (a) Air Flow of 500 Pa · s/m^2. (b) Air Flow of 1000 Pa · s/m^2.

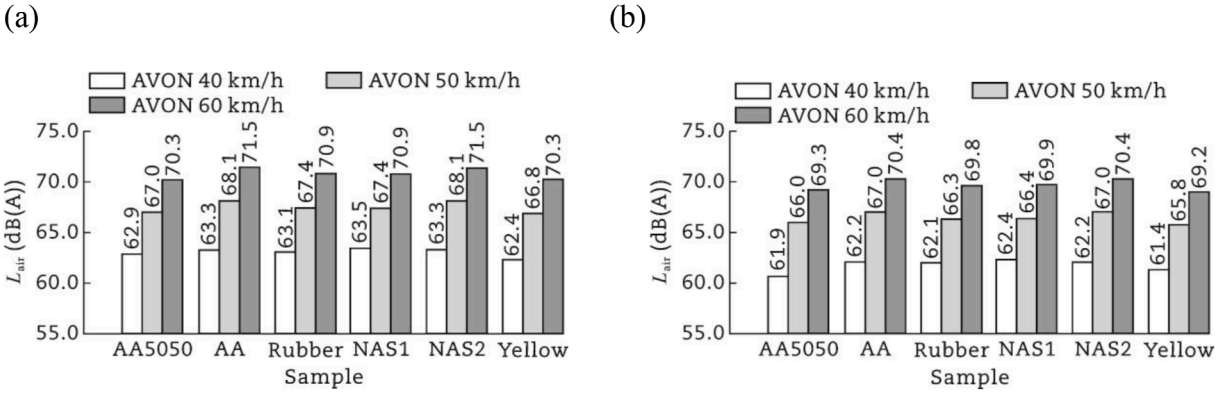

Fig. 10. L_{air} noise levels for AVON tire. (a) Air Flow of 500 Pa · s/m^2. (b) Air Flow of 1000 Pa · s/m^2.

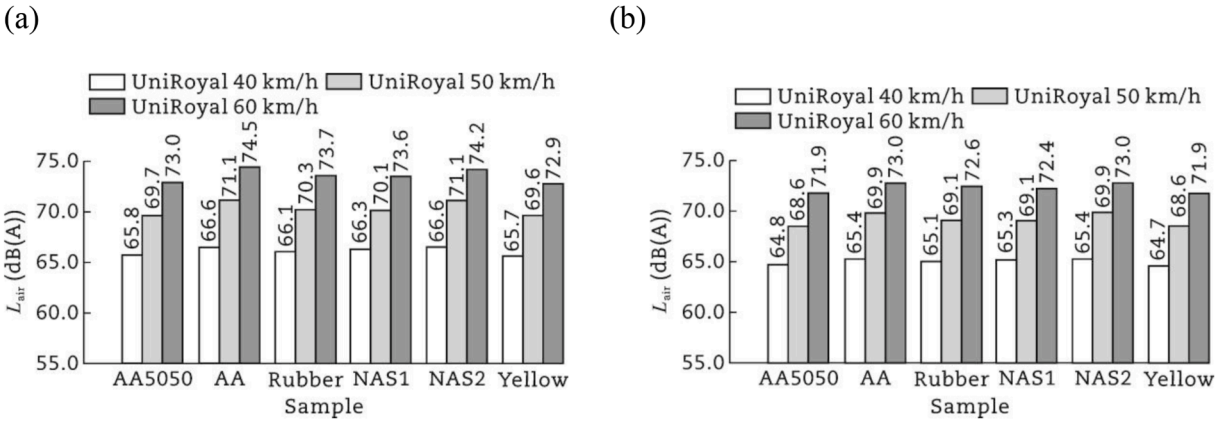

Fig. 11. L_{air} noise levels for Uniroyal tire. (a) Air Flow of 500 Pa · s/m^2. (b) Air Flow of 1000 Pa · s/m^2.

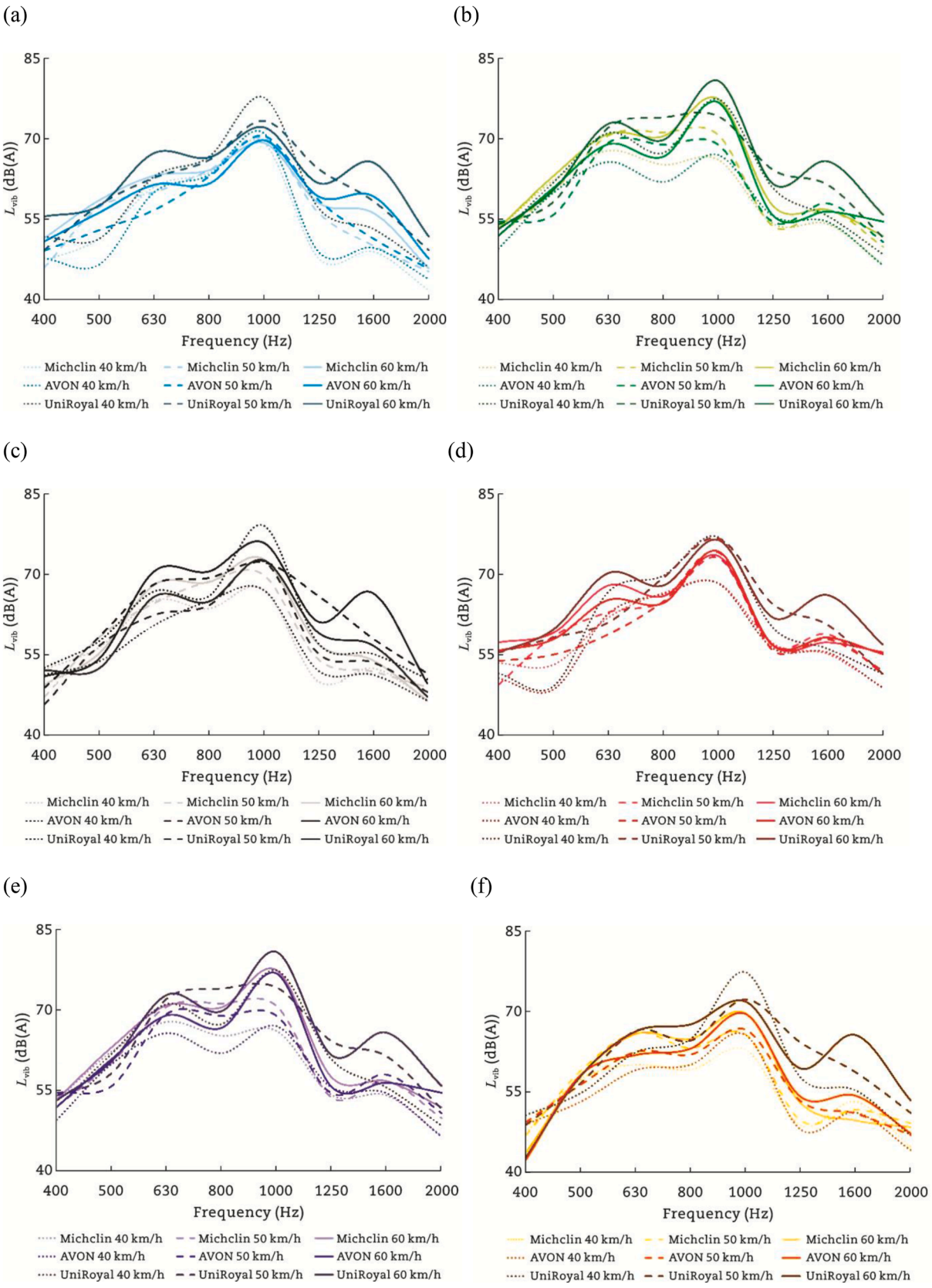

Fig. 12. L_{vib} noise spectrum (air flow 500 Pa · s/m^2) for each sample categorized by tire types and speeds. (a) Sample AA5050. (b) Sample AA. (c) Sample rubber. (d) Sample NAS1. (e) Sample NAS2. (f) Sample Yellow.

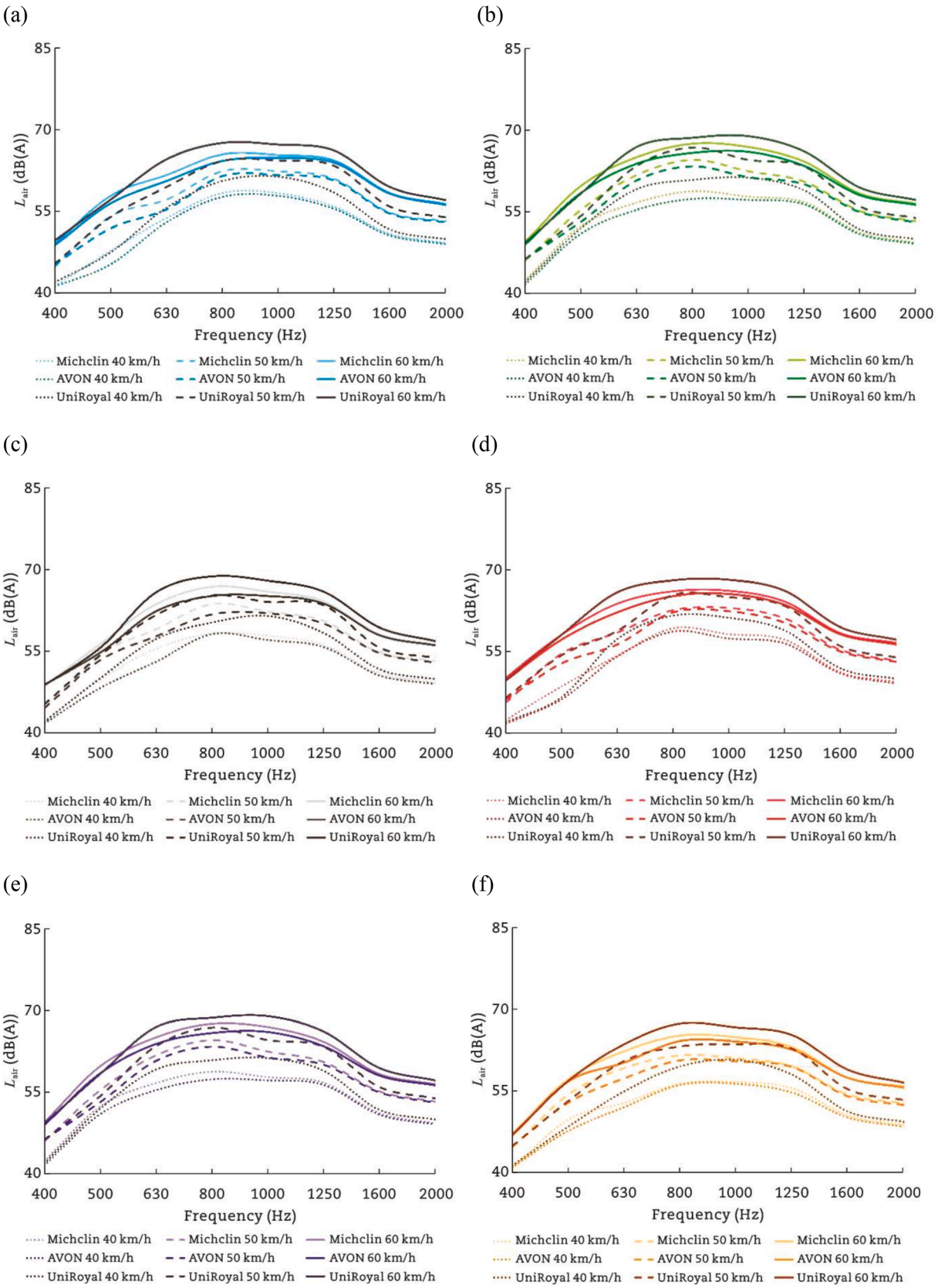

Fig. 13. L_{air} noise spectrum (air flow 500 Pa · s/m^2) for each sample categorized by tire types and speeds. (a) Sample AA5050. (b) Sample AA. (c) Sample rubber. (d) Sample NAS1. (e) Sample NAS2. (f) Sample Yellow.

figures are presented for an air flow resistance of 500 Pa · s/m^2 for the sake of simplicity. In these two figures, it is possible to note that the noise levels are higher in the range between 800 and 1250 Hz and that the speed plays a major role, especially for L_{air} noise.

Fig. 12 clearly demonstrates that the vibro-dynamic component of rolling noise exhibits higher spectral values at frequencies below 1 kHz, showing a peak at 1000 Hz, and this aligns with the expected frequency range for this phenomenon. Moreover, as the MPD of the mixtures increases, there is a corresponding amplification of the vibratory phenomenon, similar to that observed in open graded friction course. Interestingly, at high speeds (i.e., 60 km/h), all mixtures, regardless the tire type, exhibit two distinct peaks in the spectrum at 630 and 1000 Hz, respectively. Notably, UniRoyal tires present a third peak at frequencies significantly higher than the typical range of vibro-dynamic phenomena (i.e., at 1630 Hz), despite its lower amplitude compared to the previous peaks.

Fig. 12 indicates that the Yellow and AA5050 mixes exhibit lower L_{vib} levels across all frequencies compared to the other samples, for fixed speeds and tire types. In contrast, NAS2 and AA samples again have higher levels in most frequencies and they show an almost identical pattern, consistently with the previous data examined, followed by NAS1. The rubber mixture exhibits an interesting behaviour, with its spectral profile falling approximately halfway between the previous ones.

Regardless the aerodynamic noise, the results are presented in Fig. 13. In this case, the spectra exhibit a vertical mirroring effect compared to the vibro-dynamic phenomenon, with higher values corresponding to frequencies above 1 kHz (aerodynamic domain) and lower values to frequencies below. Moreover, L_{air} spectra demonstrates a linear increase in sound pressure with increasing speed from 40 to 60 km/h, which is approximately constant for all the frequencies and attributable to the shift into the speed range dominated by the aerodynamic phenomena. Finally, no peaks are detected for all the samples and tires type.

With respect to the samples, at medium and low frequencies, the NAS2, NAS1 and AA, appear to have overall higher noise levels. The rubber has mid-range noise level at all frequencies independently of the speed. In contrast, the Yellow and AA5050 have lower levels of noise.

3.5. Noise levels by modelling per texture indicators: comparative analysis

Tables 4 and 5 present the correlation matrixes (Pearson correlation coefficient) identified between the texture indicators and the tire-vibration noise (L_{vib}) and aerodynamic noise (L_{air}), respectively. To facilitate data presentation, a coding system denoted by *X_a_b* is employed, where '*X*' represents the tire type (M: Michelin; A: AVON; UR: UniRoyal), *a* represents the vehicle speed (40, 50, and 60 km/h), and *b* indicates the air flow resistance (500 and 1000 Pa · s/m^2).

In the case of tire-vibration noise (L_{vib}), it is possible to note that the texture indicators MPD, R_z, and RMS reveal a positive correlation with the L_{vib} values. Furthermore, these correlations are strong at higher speeds (i.e., 50 and 60 km/h), and this is particularly evident for AVON and UniRoyal tires, which, on the contrary, show low correlation values at 40 km/h. In general, this trend is also observed for all other texture indicators and noise-related indicators. The observed correlation suggests that the generated noise might be more attributable to the tire type (stiffness of the rubber) for a given speed rather than the surface texture conformation.

The shape of the heights' distribution of the profile, z_i, has a certain impact on rolling noise. Road surfaces with a distribution that tends towards lower values compared to the average profile value and is more concentrated around the profile mean exhibit lower rolling noise. This observation is supported by the positive correlation between vibro-dynamic noise and skewness, R_{sk}, and the negative correlation with kurtosis, R_{ku}. On the other hand, the END_T indicator does not show a significant correlation with L_{vib} values, except at lower speeds (i.e., 40 km/h) and with AVON tire only. This justifies the transition to the *g*-factor in the new ISO 10844 standard. The *g*-factor exhibits a negative correlation with tire-vibration noise, typically exceeding 0.85 (except for AVON and UniRoyal tires at low speeds). As mentioned previously, an increase in the *g*-factor corresponds to a road surface with a less tendency in producing rolling noise.

Reading Table 5, no significant trends or differences are observed between the various tires and different speeds, further supporting the previous hypothesis: different tire types influence aerodynamic and vibration phenomena in distinct ways (Beckenbauer et al., 2008). In this case, the considerations made previously regarding the most common texture indicators and the shape of the profiles' distribution also apply, revealing quite higher positive correlations. With respect to noise-related indicators, the correlation between L_{air} values and the END_T indicator is completely absent, but remains very strong in the case of the *g*-factor. Therefore, given the boundary condition of the present research and the soundness of the modelling with SPERoN® proven in several research, in the absence of further tools for noise assessment, analysis using a laser profilometer and calculation of the *g*-factor by using a bearing area curve (Abbott curve) can provide good information regarding the possible rolling noise generated at the tire/road contact.

Table 4
Correlation matrix between L_{vib} and surface texture indicators.

L_{vib}	MPD	R_z	RMS	R_{sk}	R_{ku}	END_T	*g*-factor
M_40_500	0.802	0.805	0.840	0.778	−0.874	0.562	−0.901
M_40_1000	0.808	0.812	0.849	0.784	−0.882	0.551	−0.905
M_50_500	0.927	0.984	0.862	0.940	−0.933	0.130	−0.964
M_50_1000	0.923	0.990	0.860	0.933	−0.926	0.107	−0.952
M_60_500	0.877	0.985	0.794	0.881	−0.845	−0.042	−0.866
M_60_1000	0.870	0.981	0.785	0.874	−0.835	−0.061	−0.854
A_40_500	0.492	0.415	0.524	0.480	−0.573	0.788	−0.657
A_40_1000	0.494	0.415	0.538	0.480	−0.584	0.787	−0.657
A_50_500	0.857	0.850	0.940	0.854	−0.974	0.275	−0.911
A_50_1000	0.867	0.867	0.945	0.862	−0.978	0.275	−0.919
A_60_500	0.914	0.989	0.811	0.940	−0.893	−0.026	−0.928
A_60_1000	0.913	0.990	0.813	0.936	−0.892	−0.024	−0.925
UR_40_500	0.639	0.694	0.897	0.518	−0.785	0.679	−0.668
UR_40_1000	0.439	0.592	0.798	0.261	−0.576	0.349	−0.336
UR_50_500	0.916	0.941	0.744	0.985	−0.887	−0.034	−0.973
UR_50_1000	0.919	0.949	0.753	0.983	−0.890	−0.031	−0.971
UR_60_500	0.884	0.989	0.808	0.884	−0.858	−0.012	−0.876
UR_60_1000	0.882	0.989	0.814	0.881	−0.859	−0.018	−0.871

Table 5
Correlation matrix between L_{air} and surface texture indicators.

L_{air}	MPD	R_z	RMS	R_{sk}	R_{ku}	END_T	g-factor
M_40_500	0.914	0.948	0.903	0.915	−0.960	0.266	−0.970
M_40_1000	0.905	0.928	0.917	0.904	−0.968	0.292	−0.965
M_50_500	0.827	0.963	0.785	0.798	−0.795	0.028	−0.799
M_50_1000	0.863	0.979	0.800	0.848	−0.833	0.064	−0.857
M_60_500	0.832	0.963	0.761	0.821	−0.791	−0.075	−0.798
M_60_1000	0.836	0.966	0.779	0.822	−0.803	−0.074	−0.800
A_40_500	0.849	0.818	0.888	0.866	−0.953	0.310	−0.931
A_40_1000	0.817	0.786	0.900	0.817	−0.942	0.375	−0.897
A_50_500	0.876	0.982	0.792	0.871	−0.841	0.059	−0.879
A_50_1000	0.887	0.981	0.780	0.896	−0.847	0.053	−0.902
A_60_500	0.881	0.987	0.816	0.881	−0.860	−0.046	−0.865
A_60_1000	0.904	0.994	0.834	0.911	−0.891	0.000	−0.906
UR_40_500	0.921	0.989	0.821	0.947	−0.905	−0.004	−0.941
UR_40_1000	0.930	0.972	0.882	0.955	−0.958	0.022	−0.954
UR_50_500	0.834	0.964	0.761	0.816	−0.789	0.013	−0.814
UR_50_1000	0.855	0.970	0.744	0.861	−0.802	−0.056	−0.843
UR_60_500	0.919	0.990	0.832	0.869	−0.828	0.013	−0.857
UR_60_1000	0.882	0.989	0.814	0.881	−0.859	−0.018	−0.871

Nevertheless, it is crucial to emphasize that these approaches fail to consider the potential sound absorption characteristics of the materials (porosity, presence of sound-absorbing materials), thereby diminishing the representativeness of the analysis for such types of mixtures.

4. Conclusions

This study focused on evaluating the rolling noise performance of various microsurfacing mixtures, incorporating both natural and artificial aggregates, as well as different binders and particle size distributions. Using a combination of 2D texture analysis and the SPERoN® noise prediction model, the research explored the relationships between tire/road noise levels and surface texture indicators. These findings enhance the understanding of noise generation mechanisms in pavement engineering, offering insights applicable beyond microsurfacing to other pavement types.

Given the boundaries of this research, the results demonstrate that the use of different aggregates and particle size distribution can contribute and influence the noise performance. Specifically, the use of lower NMAS (i.e., Yellow) and high percentages of uniformly shaped AEAs (i.e., AA5050) were found to reduce rolling noise levels effectively. Thus, discontinuous particle size distributions could also play a crucial role in this sense. On the other hand, the presence of AEAs in substitution of natural aggregates but in low percentages, probably contributes to increment the heterogeneity of the mixture and the resulting texture: in fact, mixture AA exhibited the worst behaviour among all mixtures, looking at both approaches. The Rubber mixture has a midlevel noise behavior and the results could be also better due to the sound–absorption properties of crumb rubber.

Additionally, the distribution of profile height (z_i) significantly influences rolling noise. In fact, surface profiles characterized by negative skewness and positive kurtosis exhibited lower tendencies for noise generation. These findings also underscore the limitations of traditional indicators like END_T, emphasizing the *g*-factor derived from the Abbott curve as a more reliable and strongly correlated predictor of pavement noise levels (i.e., L_{vib} and L_{air} from SPERoN®), with ease of calculation.

The limitations of this study are primarily attributed to practical constraints related to the use of the software and other factors generally associated with noise generation and absorption mechanisms. These include the use of 2D profiling tools, which, while effective, may not fully capture the complexity of three-dimensional surface textures, as well as the exclusion of acoustic impedance and material porosity, which are integral to noise absorption.

Future research should build on these findings by employing 3D surface texture analyses for a deeper understanding of texture-noise relationships and incorporating acoustic impedance measurements of the materials. Moreover, field validations of the laboratory findings would strengthen the applicability of these results to real-world pavement design and performance optimization. These findings offer valuable insights for road engineering, supporting the design of low-noise pavements and emphasizing the potential of artificial aggregates as sustainable and effective alternatives to natural materials.

CRediT authorship contribution statement

Sérgio Copetti Callai: Investigation, Conceptualization, Writing – original draft, Software, Methodology. **Manuel De Rose:** Writing – review & editing, Methodology, Software, Data curation, Investigation. **Beate Altreuther:** Data curation, Writing – review & editing, Methodology, Software. **Rosolino Vaiana:** Supervision, Writing – review & editing. **Cesare Sangiorgi:** Writing – review & editing, Supervision, Conceptualization.

Declaration of competing interest

The authors do not have any conflict of interest with other entities or researchers.

Acknowledgments

This research was funded by the European Union's Horizon 2020 research and innovation program under the Marie Sklodowska-Curie grant agreement N°765057 (SAFERUP Project).

References

Altreuther, B., Maennel, M., 2018. Low noise pavements in Germany: established concepts and new ideas. In: 2018 Joint Conference-Acoustics, Ustka, 2018.
Alves, S., Maennel, M., 2016. Application of Speron to the development of low noise road surfaces. In: EuroRegio2016, Porto, 2016.
Beckenbauer, T., Klein, P., Hamet, J.F., et al., 2008. Tyre/road noise prediction: a comparison between the SPERoN and HyRoNE models–part 1. Journal of the Acoustical Society of America 123, 3388.
Beckenbauer, T., Kuijpers, A., 2001. Prediction of pass-by levels depending on road surface parameters by means of a hybrid model. In: INTER-NOISE and NOISE-CON Congress and Conference, Hague, 2001.
Berge, T.S., Haukland, F., Ustad, A., 2009. Environmental Friendly Pavements. Results from Noise Measurements 2005–2008. SINTEF Report A9721. SINTEF, Trondheim.
Beutel, M.E., Brähler, E., Ernst, M., et al., 2020. Noise annoyance predicts symptoms of depression, anxiety and sleep disturbance 5 years later. Findings from the Gutenberg health study. The European Journal of Public Health 30 (3), 516–521.
Bhargava, N., Siddagangaiah, A.K., Ryntathiang, T.L., 2020a. State of the art review on design and performance of microsurfacing. Road Materials and Pavement Design 21, 2091–2125.
Bhargava, N., Siddagangaiah, A.K., Ryntathiang, T.L., 2020b. Reliability of microsurfacing mix subjected to variation in aggregate gradation. Transportation Research Record 2674, 720–730.
Boscaino, G., Pratico, F.G., 2001. Classification and inventory of indicators of pavement surface texture. Bulletin des Laboratoires des Ponts et Chaussees 234 (2001), 17–34.

Callai, S.C., De Rose, M., Tataranni, P., et al., 2022. Microsurfacing pavement solutions with alternative aggregates and binders: a full surface texture characterization. Coatings 12, 1905.
Canestrari, F., Pasquini, E., Ferrotti, G., et al., 2009. Experimental Study on Cold Micro-surfacing with Crumb Rubber. Transportation Research Board, Washington DC.
Chen, D., Ling, C., Wang, T., et al., 2018. Prediction of tire-pavement noise of porous asphalt mixture based on mixture surface texture level and distributions. Construction and Building Materials 173, 801–810.
Chen, L., Cong, L., Dong, Y., et al., 2021. Investigation of influential factors of tire/pavement noise: a multilevel Bayesian analysis of full-scale track testing data. Construction and Building Materials 270, 121484.
Chen, S., Liu, X., Luo, H., et al., 2022. A state-of-the-art review of asphalt pavement surface texture and its measurement techniques. Journal of Road Engineering 2 (2), 156–180.
Chen, W., Zheng, M., Wang, H., 2021. Evaluating the tire/pavement noise and surface texture of low-noise micro-surface using 3D digital image technology. Frontiers in Materials 8, 683947.
Christensen, J.S., Hjortebjerg, D., Raaschou-Nielsen, O., et al., 2016. Pregnancy and childhood exposure to residential traffic noise and overweight at 7 years of age. Environment International 94, 170–176.
Copetti Callai, S., Tataranni, P., De Rose, M., et al., 2022. A preliminary laboratory evaluation of artificial aggregates from alkali-activated basalt powder. Sustainability 14, 16653.
De Rose, M., Iuele, T., Perri, G., et al., 2023. On the mix design advances in microsurfacing: a systematic surface performance-oriented literature review. International Journal of Pavement Research and Technology 2023, 004077.
Del Pizzo, L.G., Teti, L., Moro, A., et al., 2020. Influence of texture on tyre road noise spectra in rubberized pavements. Applied Acoustics 159, 107080.
Descornet, G., 2006. Silvia–sustainable road surfaces for traffic noise control. In: Transport Research Arena Europe, Göteborg, 2006.
Dreger, S., Schüle, S.A., Hilz, L.K., et al., 2019. Social inequalities in environmental noise exposure: a review of evidence in the WHO European region. International Journal of Environmental Research and Public Health 16 (6), 1011.
Eelco den Boer, L.C., Schroten, A., 2007. Traffic Noise Reduction in Europe. CE Delft, Delft.
European Comission, 2017. Report from the Commission to the European Parliament and the Council on the Implementation of the Environmental Noise Directive in Accordance with Article 11 of Directive 2002/49/EC. European Comission, Brussels.
European Environment Agency, 2020. Environmental Noise in Europe–2020. European Environment Agency, Copenragen.
Forssén, J., Hoffmann, A., Kropp, W., 2018. Auralization model for the perceptual evaluation of tyre-road noise. Applied Acoustics 132, 232–240.
German-French Cooperation P2RN, 2009. DEUFRAKO–P2RN: Prediction and Propagation of Rolling Noise. German Federal Ministry of Economy and Technology, Berlin.
Gottaut, C., Goubert, L., 2016. Texture-based Descriptors for Road Surface Properties and How They Can Be Used in the Appropriate Standards. Project ROSANNE: Rolling Resistance, Skid Resistance, and Noise Emission Measurement Standards for Road Surfaces. European Commission, Brussels.
Goubert, L., Bendtsen, H., Bergiers, A., et al., 2016. The poroelastic road surface (PERS): is the 10 dB reducing pavement within reach? In: Torrenti, J., La Torre, F. (Eds.), Materials and Infrastructures 1. Wiley, pp. 253–268.
Grilli, A., Graziani, A., Carter, A., et al., 2019. Slurry surfacing: a review of definitions, descriptions and current practices. RILEM Technical Letters 4, 103–109.
Hoffmann, A., Kropp, W., 2019. Auralization of simulated tyre noise: psychoacoustic validation of a combined model. Applied Acoustics 145, 220–227.
ISO, 2002. Characterization of Pavement Texture by Use of Surface Profiles. Part 3: Specifications and Classification of Profilometers, 2002. ISO 13473-3. ISO, Geneva.
ISO, 2014. Acoustics–Specification of Test Tracks for Measuring Sound Emitted by Road Vehicles and Their Tyres, 2014. ISO 10844:2014. ISO, Geneva.
ISO, 2019. Characterization of Pavement Texture by Use of Surface Profiles. Part 1: Determination of Mean Profile Depth, 2019. ISO 13473-1. ISO, Geneva.
ISO, 2021. Acoustics–Specification of Test Tracks for Measuring Sound Emitted by Road Vehicles and Their Tyres, 2021. ISO 10844:2021. ISO, Geneva.
International Slurry Surfacing Association (ISSA), 2010. Recommended Performance Guidelines for Micro Surfacing. ISSA, Annapolis.
JRE Editorial Office, Cavalli, M.C., Chen, D., 2023. Review of advanced road materials, structures, equipment, and detection technologies. Journal of Road Engineering 3 (4), 370–468.
Klein, P., Beckenbauer, T., Hamet, J.-F., et al., 2008. Tyre/road noise prediction: a comparison between the SPERoN and HyRoNE models–part 2. Journal of the Acoustical Society of America 123, 3389.
Kleizienė, R., Šernas, O., Vaitkus, A., et al., 2019. Asphalt pavement acoustic performance model. Sustainability 11, 2938.
Kuijpers, A., Van Blokland, G., 2001. Tyre/road noise modelling: the road from a tyre's point-of-view. In: Internoise 2003, Seogwipo, 2001.
Li, H., Zhou, L., Cai, Y., et al., 2024. Potential applications for composite utilization of rubber and plastic in asphalt pavements: a critical review. Journal of Traffic and Transportation Engineering (English Edition) 11 (5), 939–971.
Li, S., Noureldin, S., Jiang, Y., et al., 2012. Evaluation of Pavement Surface Friction Treatments. Purdue University, West Lafayette.
Li, S., Xiong, R., Yu, D., et al., 2017. Friction Surface Treatment Selection: Aggregate Properties, Surface Characteristics. Alternative Treatments, and Safety Effects. Purdue University, West Lafayette.
Ling, S., Yu, F., Sun, D., et al., 2021. A comprehensive review of tire-pavement noise: generation mechanism, measurement methods, and quiet asphalt pavement. Journal of Cleaner Production 287, 125056.
Ma, C., Huang, X., Li, J., 2024. A review of research on urban parking prediction. Journal of Traffic and Transportation Engineering (English Edition) 11 (4), 700–720.
Makoundou, C., Johansson, K., Wallqvist, V., et al., 2021a. Functionalization of crumb rubber surface for the incorporation into asphalt layers of reduced stiffness: an overview of existing treatment approaches. Recycling 6, 19.
Makoundou, C., Sangiorgi, C., Johansson, K., et al., 2021b. Development of functional rubber-based impact-absorbing pavements for cyclist and pedestrian injury reduction. Sustainability 13 (20), 11283.
Mikhailenko, P., Piao, Z., Kakar, M.R., et al., 2022. Low-noise pavement technologies and evaluation techniques: a literature review. International Journal of Pavement Engineering 23, 1911–1934.
Miljković, M., Radenberg, M., 2012. Thin noise-reducing asphalt pavements for urban areas in Germany. International Journal of Pavement Engineering 13, 569–578.
Miljković, M., Radenberg, M., Gottaut, C., 2014. Characterization of noise-reducing capacity of pavement by means of surface texture parameters. Journal of Materials in Civil Engineering 26 (2), 240–249.
Münzel, T., Sørensen, M., Daiber, A., 2021. Transportation noise pollution and cardiovascular disease. Natare Reviews Cardiology 18 (9), 619–636.
Nowoświat, A., Sorociak, W., Żuchowski, R., 2020. The impact of the application of thin emulsion mat microsurfacing on the level of noise in the environment. Construction and Building Materials 263, 120626.
Patrick, S., 2018. Guidelines and Specifications for Microsurfacing. No. AP-R569-18 (2018). Austroads Publication, Austroads, Sydney.
Peeters, B., Van Loon, R., Van Blokland, G., 2024. 40 years investigating tyre/road noise at M+P. In: 10th Convention of the European Acoustics Association Forum Acusticum 2023, Turin, 2024.
Pignier, N., 2015. The Impact of Traffic Noise on Economy and Environment: A Short Literature Study: Performed within the Scope of the ECO2 Project Noise Propagation from Sustainable. The Centre for ECO2 Vehicle Design KTH Aeronautical and Vehicle Engineering Stockholm, Sweden.
Pinay, J., Unrau, H.-J., Gauterin, F., 2018. Prediction of close-proximity tire-road noise from tire cavity noise measurements using a statistical approach. Applied Acoustics 141, 293–300.
Poulikakos, L.D., Athari, S., Mikhailenko, P., et al., 2022. Effect of waste materials on acoustical properties of semi-dense asphalt mixtures. Transportation Research Part D: Transport and Environment 102, 103154.
Poulikakos, L.D., Schlatter, F., Huber, L., et al., 2024. Multi-scale mechanical and acoustic characterization of low noise pavements. Environmental Science and Pollution Research International 31 (51), 61073–61095.
Praticò, F.G., 2014. On the dependence of acoustic performance on pavement characteristics. Transportation Research Part D: Transport and Environment 29, 79–87.
Praticò, F.G., Briante, P.G., 2020. Prediction of surface texture for better performance of friction courses. Construction and Building Materials 230, 116991.
Praticò, F.G., Vaiana, R., 2015. A study on the relationship between mean texture depth and mean profile depth of asphalt pavements. Construction and Building Materials 101, 72–79.
Puzzo, L., Loprencipe, G., Tozzo, C., et al., 2017. Three-dimensional survey method of pavement texture using photographic equipment. Measurement 111, 146–157.
Pyko, A., Lind, T., Mitkovskaya, N., et al., 2018. Transportation noise and incidence of hypertension. International Journal of Hygiene and Environmental Health 221, 1133–1141.
Rahmani, S., Mousavi, S.M., Kamali, M.J., 2011. Modeling of road-traffic noise with the use of genetic algorithm. Applied Soft Computing 11, 1008–1013.
Sangiorgi, C., Bitelli, G., Lantieri, C., et al., 2012. A study on texture and acoustic properties of cold laid microsurfacings. Procedia - Social and Behavioral Sciences 53, 223–234.
Tayebi, N., Polycarpou, A.A., 2004. Modeling the effect of skewness and kurtosis on the static friction coefficient of rough surfaces. Tribology International 37, 491–505.
Teti, L., De León, G., Del Pizzo, L.G., et al., 2020. Modelling the acoustic performance of newly laid low-noise pavements. Construction and Building Materials 247, 118509.
Vaiana, R., De Rose, M., Perri, G., 2023. Microsurfacing: a predictive macrotexture model from mix design parameters. Construction and Building Materials 409, 133961.
Van Blokland, G., Schwanen, W., 2012. Requirements and testing methods for ISO 10844: 2011 test tracks. In: INTER-NOISE and NOISE-CON Congress and Conference, New York City, 2012.
Vázquez, V.F., Terán, F., Paje, S.E., 2020. Dynamic stiffness of road pavements: construction characteristics-based model and influence on tire/road noise. Science of The Total Environment 736, 139597.
Vieira, T., Sandberg, U., Erlingsson, S., 2021. Negative texture, positive for the environment: effects of horizontal grinding of asphalt pavements. Road Materials and Pavement Design 22, 1–22.
Xu, L., Lu, T., Chen, Z., et al., 2024. A review of polyurethane as an alternative to asphalt binder for more sustainable roads: performance, environment, and economy. Journal of Traffic and Transportation Engineering (English Edition) 11 (6), 268–1290.

Zakerzadeh, M., Shahbodagh, B., Ng, J., et al., 2024. The use of waste tyre rubber in Stone Mastic Asphalt mixtures: a critical review. Construction and Building Materials 418, 135420.
Zhan, W., Huang, P., 2019. Modeling tangential contact based on non-Gaussian rough surfaces. Proceedings of the Institution of Mechanical Engineers - Part J: Journal of Engineering Tribology 233, 51–60.
Zhang, Y., Tayarani, M., Wang, S., et al., 2021. Identifying urban built environment factors in pregnancy care and maternal mental health outcomes. BMC Pregnancy and Childbirth 21, 599.

Sérgio Copetti Callai is group leader of the road surface properties team at the Institute of Highway Engineering (ISAC), RWTH Aachen, Germany. He received his PhD from the University of Bologna as a Marie Skłodowska-Curie Fellow, following a master's degree in transportation engineering from the University of São Paulo (USP), supported by a CAPES scholarship, and a bachelor's degree in civil engineering from UNIJUÍ. He has experience in both industry and academia, including a research position at the University of Coimbra. His research focuses on pavement surface characteristics, encompassing texture analysis, skid resistance, noise reduction, sustainable materials, and AI-based solutions for safe and comfortable road design.

Manuel De Rose is a post-doctoral researcher at the University of Calabria, Italy. He received his PhD in civil and industrial engineering from the same institution in 2024, following the completion of his master degree in transportation engineering in 2020. His research focuses on pavement surface characteristics and environmental sustainability in road pavements, encompassing: recycling techniques for waste materials in bituminous mixtures, the development and optimization of bio-binders as bitumen substitutes, cold bituminous asphalt treatments, and life cycle assessment for environmental impact evaluation. He has recently undertaken a research period at the University of Minho, Portugal.

Beate Altreuther is a senior consultant at Müller-BBM Industry Solutions for noise and vibrations, with focus on traffic noise, low noise road surfaces, urban sound planning. Advising clients from the public and private sectors on noise protection against road traffic noise as well as designing, carrying out and evaluating measurements of acoustically relevant parameters on roadways; urban sound planning for the design of an acoustically high-quality environment. Collaboration in national and international research projects on “reduction of tyre road noise”, e.g., Quiet Road Traffic (D), SONORUS and SaferUP! (EU). Project coordination of several research projects on the topic of low noise concrete road surfaces and on the CPX measurement method.

Rosolino Vaiana is an associate professor at the Department of Civil Engineering of the University of Calabria. His primary research activity addresses the themes related to road pavement materials, characterization of road surface performance (friction, drainability, rolling noise etc), and construction technology, exploring the use of recycled materials and low-impact solutions. Moreover, he developed two main research topics in the field of road design: one is related to the functional and geometric study of roundabout junctions by traffic microsimulation software; the other is about road safety and driver behavior. At the University of Calabria, Rosolino Vaiana performs teaching activities since 2005 about these subjects: foundations of road infrastructures (bachelor's degree in civil engineering) and Road pavement design and maintenance (master's degree in civil engineering). He was and is currently a PhD thesis supervisor.

Cesare Sangiorgi is a full professor at the University of Bologna, and he specializes in pavement engineering materials and sustainable construction technologies, prioritizing recycled materials and low-impact solutions. He fosters student engagement through collaborations with esteemed research institutes. Since 2001, he's partnered with the Nottingham Transportation Engineering Centre and expanded collaborations globally. Prof. Sangiorgi led SaferUP!, recruiting 15 early stage researchers in a consortium of 30 for sustainable urban pavement projects. Presently, he coordinates GreeNexUS, a HORIZON EUROPE project promoting urban greening and infrastructure safety. With numerous research agreements nationally and internationally, he actively contributes to professional associations like SIIV, APSE, iSMARTi, and RILEM, and serves on journal boards and conference committees, publishing extensively in pavement engineering.